Available online at www.sciencedirect.com
ScienceDirect
Journal of Power Sources 169 (2007) 361–368
JOURNAL OF POWER SOURCES
www.elsevier.com/locate/jpowsour

Review

The effect of sorbitol on the morphological characteristics of lead–tin films electrodeposited from an alkaline bath

J.L.P. Siqueira, I.A. Carlos *

Departamento de Química, Universidade Federal de São Carlos, CP 676, 13565-905 São Carlos, SP, Brazil

Received 2 February 2007; received in revised form 19 March 2007; accepted 29 March 2007
Available online 10 April 2007

Abstract

An alkaline Pb–Sn plating bath containing sorbitol as additive has been developed, which has the advantage of low toxicity and ease of handling relative to fluoborate baths, etc. The Pb–Sn deposition voltammetric curve from this bath revealed two deposition processes, at −0.87 and −1.17 V. The voltammetric studies at various sweep rates indicate that the Pb–Sn deposition process is controlled by mass transport. The joint diffusion coefficient of the Pb(II) and Sn(II) sorbitate complex species is 1.15×10^{-6} cm^2 s^{-1}. SEM analysis showed that the films produced at −0.87 and −1.17 V are, respectively, composed of dendritic or hexagonal crystals, showing that co-deposition of tin hindered dendritic growth. EDS of the Pb–Sn films showed that the deposit obtained at −0.87 V is pure lead, while that at −1.17 V, with 5.0 or 10.0 C cm^{-2}, has 19.10 wt% Sn or 26.35 wt% Sn, respectively. It was observed that the Pb–Sn electrodeposited films were grey at both deposition potentials (−0.87 and −1.17 V) and deposition charges (5.0 and 10.0 C cm^{-2}). X-ray spectra showed that at the potential −0.87 V a mixture of Pb, $PbPt_4$ and Pb_2PtO_4 were deposited, while at −1.17 V, Pb, β-Sn, and $PbSnO_3$ were deposited.

Keywords: Lead–tin; Electrodeposition; Sorbitol–alkaline bath; X-ray spectroscopy; Morphology

Contents

1. Introduction 361
2. Experimental 362
3. Results and discussion 362
   3.1. EDS analysis of the Pb–Sn deposits 365
   3.2. X-ray analysis of the Pb–Sn deposits 366
   3.3. Scanning electronic microscopy 367
4. Conclusions 368
   Acknowledgements 368
   References 368

1. Introduction

Lead–tin alloys have been widely used in industry as: corrosion resistant coatings for steel, which usually contains 4–10% Sn; surface layers on bearings, consisting of 7–10% Sn, solderable coatings for the assembly of electronic equipment, where the alloys contain 10–60% Sn [1]. In lead–acid batteries, lead–tin alloys have been used to overcome the passivation problems following the replacement of the traditional Pb–Sb grids with antimony-free or low antimony alloys.

Pavlov [2] reports that when the lead–antimony grids in lead/acid batteries were substituted by lead–calcium ones, battery cycle life was dramatically shortened. Pavlov called this phenomenon "premature capacity loss" (PCL). The changes in

* Corresponding author. Tel.: +55 16 33518067; fax: +55 16 33518350.
E-mail address: diac@power.ufscar.br (I.A. Carlos).

0378-7753/$ – see front matter © 2007 Elsevier B.V. All rights reserved.
doi:10.1016/j.jpowsour.2007.03.058

the electrical properties of the corrosion layer on grid are the reason for the PCL effect, which is due to: (i) formation of a $PbSO_4$ barrier layer and (ii) formation of a α-PbO semiconductor layer.

Studies indicate that alloying with tin makes the PbO layer thinner, promotes the oxidation of this oxide to PbO_n ($1 < n < 2$), which leads to diminishing the amounts of PbO_2. Then, this sets a limit for the optimum concentration of tin in the alloy, i.e., high enough concentration to prevent the formation of an insulating PbO phase at the grid surface, but low enough to avoid hindrance of PbO_2 formation [3].

Deposition baths for Pb–Sn described in the literature have fluosilicate, fluoborate or sulphamate as components. However, these electrolytes have limitations, such as corrosiveness, the need for various additives, etc. [1–8]. Moreover, they are incompatible with modern standards, due to difficult handling and the need for costly industrial wastewater treatment for correct disposal into the environment. In order to develop an alternative Pb–Sn plating bath, we have studied an alkaline bath with added sorbitol. The choice of this bath resides in the fact that the presence of the organic additive sorbitol has led to acceptable copper and copper alloy, nickel, lead, zinc and iron–zinc alloy deposits, this additive acting as an effective grain refiner in both acid and alkaline plating [9–17].

Accordingly, this paper illustrates how the deposition conditions influence the alloy composition, surface morphology, current efficiency and structure of Pb–Sn electrodeposits.

2. Experimental

All chemicals were analytical grade. Double-distilled water was used throughout. Each electrochemical experiment was performed in a freshly prepared alkaline bath, containing 0.05 M $Pb(NO_3)_2$ and/or 0.05 M $SnCl_2$, 0.8 M NaOH and 0.4 M sorbitol ($C_6H_{14}O_6$). In this plating bath, plumbite and stannite anions are stabilized by sorbitate anions, which hinder their decomposition to PbO and SnO_2, respectively [10,17]. A Pt disk (0.196 cm^2), a Pt plate and an Hg |HgO| NaOH (1.0 M) electrode with an appropriate Luggin capillary were employed as working, auxiliary and reference electrodes, respectively. Immediately prior to the electrochemical measurements, the Pt working electrode was ground with 0.3 μm alumina, immersed in concentrated sulphuric–nitric acid solution and then rinsed with deionized water. Potentiodynamic curves were recorded with a PAR electrochemical system consisting of a model 173 potentiostat/galvanostat, at a scanning rate of 10 mV s^{-1}. All experiments were carried out at room temperature (25 °C). Potentiostatic deposits were produced at 5.0 and 10.0 C cm^{-2}. Measurements of deposition charges were recorded with an EG&G model 379 coulometer.

X-ray diffraction patterns were produced with filtered Cu Kα radiation (1.54051 Å), using a Rigaku Rotaflex RU 200B X-ray goniometer. The diffraction experiment was done with a 2θ scan (fixed $\omega = 2°$).

Scanning electron microscopy (SEM) photographs were taken with a XL 30-FEG. Energy-dispersive X-ray spectroscopy (EDS) was performed with an eLX Oxford, EDS Si/Li, Be ultrathin window.

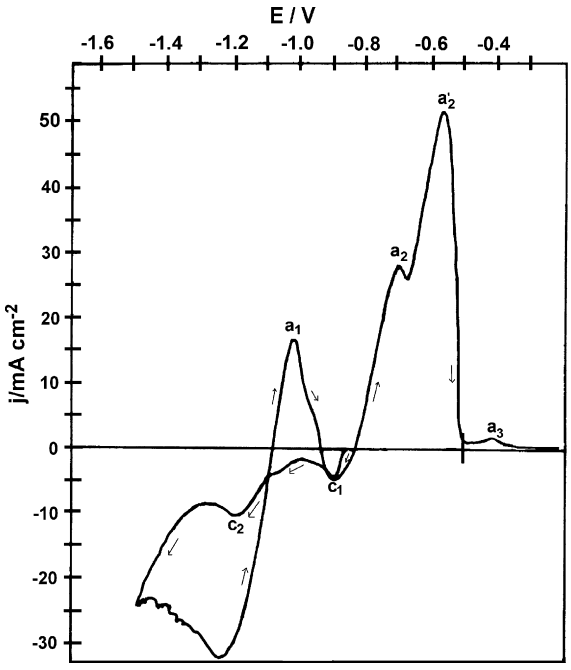

Fig. 1. Voltammetric curves for platinum substrate in 0.05 M $Pb(NO_3)_2$ + 0.05 M $SnCl_2$ + 0.4 M sorbitol and 0.8 M NaOH, at 10 mV s^{-1}. Initial potential: −0.5 V; sweep reversal potential: 1.6 V and final potential: −0.2 V.

3. Results and discussion

Fig. 1 shows a typical voltammogram for the stationary platinum electrode in the Pb–Sn plating bath containing 0.05 M $Pb(NO_3)_2$ + 0.05 M $SnCl_2$ + 0.8 M NaOH and 0.4 M sorbitol ($C_6H_{14}O_6$). The main features of this voltammogram are two cathodic peaks c_1 (∼10 mC cm^{-2}, peak potential (E_p) ∼ −0.87 V) and c_2 (∼40 mC cm^{-2}, E_p ∼ −1.17 V) and the anodic processes a_1, a_2, a'_2 and a_3. The increase in the current density at potentials more negative than −1.35 V is related to H_2 evolution.

The reactions occurring in each cathodic process were identified by recording voltammetric curves for each metal ion separately under the same conditions (Figs. 2 and 3).

Fig. 2(a) shows voltammograms recorded for the Pt substrate, with the Pb salt alone (broken line) or together with the Sn salt (solid line) in the plating solution. As can be seen, the Pb deposition (broken line) begins beyond −0.80 V (see Fig. 2(b)). Fig. 2(c) shows that before −0.80 V, lead is not deposited, and the anodic peak at ∼−0.30 V and the shoulder at ∼+0.20 V correspond to oxidation of sorbitol, as can be seen better in Fig. 2(d). Fig. 2(d) shows the potentiodynamic curve of the Pt substrate in a solution of 0.4 M sorbitate and 0.8 M NaOH. It can be seen in the forward sweep that at ∼−0.90 V the current density increases steeply, due to hydrogen evolution, while in the anodic sweep these are two anodic peaks and a shoulder. The first anodic peak corresponds to a typical hydrogen oxidation peak and the other peak and shoulder, at more positive potentials, to oxidation of sorbitol.

Comparing Pb–Sn potentiodynamic curve (solid line) with the Pb deposition (Fig. 2(b)), the peak c_1 (−0.87 V) appears at

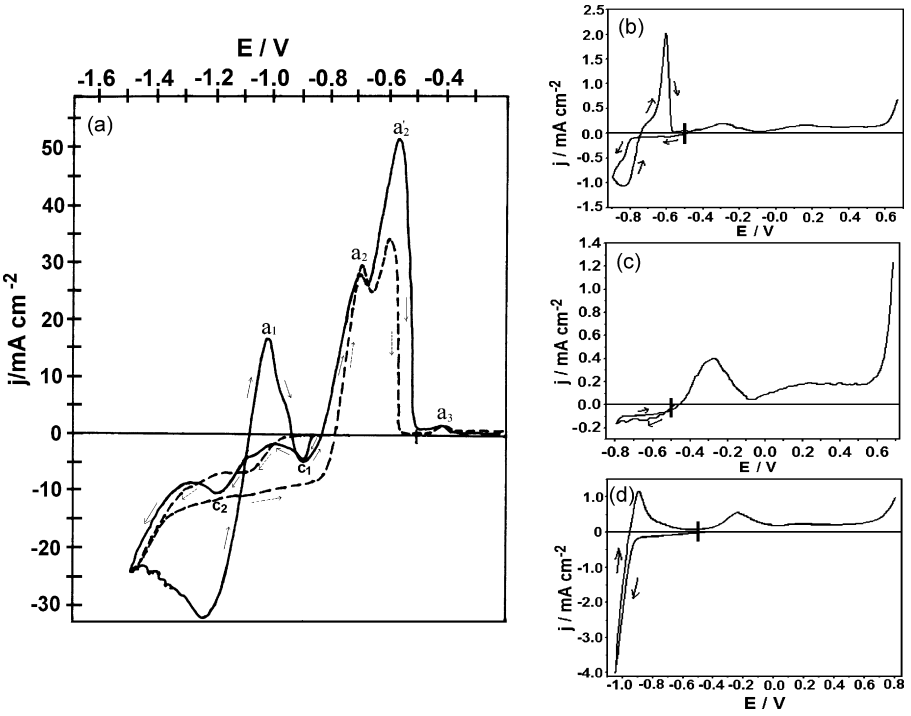

Fig. 2. Voltammetric curves for platinum substrate in: (a) 0.05 M $Pb(NO_3)_2$ + 0.05 M $SnCl_2$ + 0.4 M sorbitol + 0.8 M NaOH (—) and 0.05 M $Pb(NO_3)_2$ + 0.4 M sorbitol + 0.8 M NaOH (- - -), (b) 0.05 M $Pb(NO_3)_2$ + 0.4 M sorbitol + 0.8 M NaOH beyond −0.8 V and (c) at −0.8 V and (d) curve of Pt substrate in solution of 0.4 M sorbitol and 0.8 M NaOH $\nu = 10\,mV\,s^{-1}$. Initial potential: −0.5 V; sweep reversal potential: (a) −1.6 V; (b) −0.86 V; (c) −0.8 V; (d) −1.0 V and final potential: (a) −0.2 V; (b) 0.7 V; (c) 0.7 V; (d) 0.8 V.

a potential close to that of deposition of pure lead and can thus be associated with Pb deposition (Sections 3.1, 3.2 and 3.3).

Voltammograms recorded for the Pt substrate, using only the Sn salt (broken line) or both Pb and Sn salts (solid line) in the plating solutions, are presented in Fig. 3(a).

In the case of the Sn salt plating solution (Fig. 3(b)), when the cathodic sweep was reversed at −1.20 V, a peak of Sn dissolution can be seen in the anodic sweep. Moreover, the insert in Fig. 3(b) shows that before −1.0 V, Sn does not deposit. Comparing the tin voltammogram (Fig. 3(a), broken line) with the Pb–Sn potentiodynamic curve (Fig. 3(a), solid line), peak c_2 (−1.17 V) can probably be associated with Pb and Sn co-deposition (see Sections 3.1, 3.2 and 3.3).

Analyzing the dissolution process (Figs. 2 and 3), the first peak a_1 ($E_p = -1.0$ V) is probably related to dissolution of Pb–Sn alloy [18], while peak a_2 ($E_p = -0.70$ V) and a'_2 ($E_p = -0.60$ V) correspond to dissolution of pure Pb. Actually, the peak a_2 only forms due to undercutting of the film during dissolution.

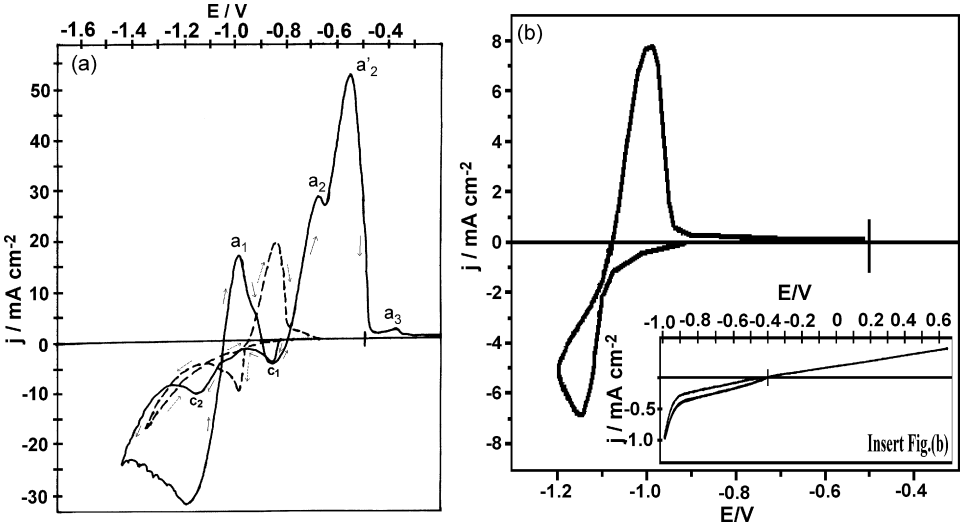

Fig. 3. Voltammetric curves for platinum substrate in: (a) 0.05 M $Pb(NO_3)_2$ + 0.05 M $SnCl_2$ + 0.4 M sorbitol + 0.8 M NaOH (—) and 0.05 M $SnCl_2$ + 0.4 M sorbitol + 0.8 M NaOH (- - -), (b) 0.05 M $SnCl_2$ + 0.4 M sorbitol + 0.8 M NaOH, $\nu = 10\,mV\,s^{-1}$. Initial potential: (a) and (b) −0.5 V; insert in (b): −0.4 V; sweep reversal potential: (a) −1.6 V; (b) −1.2 V and insert in (b) −1.0 V; final potential: (a) −0.5 V; insert in (b) 0.65 V.

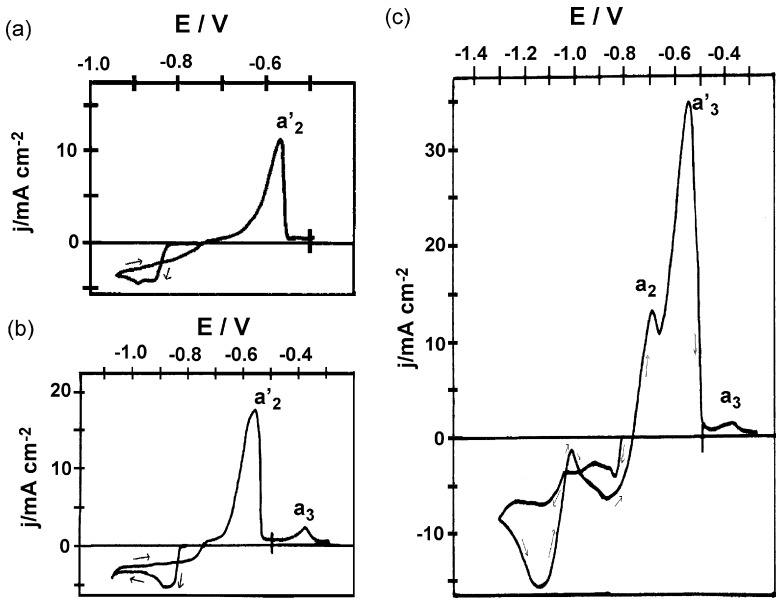

Fig. 4. Voltammetric curves for platinum substrate in 0.05 M $Pb(NO_3)_2$ + 0.05 M $SnCl_2$ + 0.4 M sorbitol + 0.8 M NaOH (—); effect of the limit potentials: (a) −0.95 V, (b) −1.1 V and (c) −1.3 V. $\nu = 10\,mV\,s^{-1}$. Initial potential: −0.5 V; final potential: (a) −0.5 V; (b) −0.3 V and (c) −0.3 V.

Peak a_3 ($E_p = -0.40$ V) corresponds to formation of lead oxide [19], which was visible to the naked eye at the end of anodic scan.

Although, for Pb–Sn alloys, there is no chemical energy of mixing, which could change the standard potentials of each phase from the values of the standard potentials of the corresponding bulk metals, there is a physical energy of dispersion of metals into such grains. This energy is expressed as a surface energy, which raises the Gibbs energy of each phase compared to that of the bulk metals and, hence, shifts the corresponding standard potential towards more negative values [18]. Comparing the potential of peak a_1 (−1.00 V) with the Sn (∼−0.85 V, Fig. 3(a)) and Pb (∼−0.70 V, Fig. 2(a)) dissolution potentials, this statement can be verified, since the potential of peak a_1 is more negative than these potentials, corroborating this assertion by Despic and Jovic [18].

Petersson and Ahlberg [20] observed two cathodic and two anodic peaks during voltammetric electrodeposition of Pb–Sn on a gold substrate, from a fluoborate bath containing 0.01 M Pb^{2+} and 0.01 M Sn^{2+}. The authors reported that the cathodic peak at more negative potential contains contributions from both lead and tin deposition and the small ones at more positive potentials are related to substrate interactions.

To characterise the cathodic process better in the region of peaks c_1 and c_2, the sweep was reversed at several limit potentials (E_f) (Fig. 4). During the dissolution process (Fig. 4), anodic peaks a_2, a_2' and a_3 were observed. Peak a_2' increases with the amount of deposited metal, which rises as the cathodic sweep was reversed at more and more negative potentials. The features of the anodic processes, when the sweep scan was reversed at $E_f = -0.95$ V (Fig. 4(a)) or −1.10 V (Fig. 4(b)) or −1.30 V (Fig. 4(c)), are similar to those of Fig. 2(a) (broken line), especially for $E_f = -1.30$ V. For this limit potential, the amount of Pb–Sn film deposited leads to undercutting of the film during the anodic sweep, forming peak a_2. Furthermore, in the voltammograms of Fig. 4, distinct cathodic processes can be seen with different values of E_f. When the sweep was reversed at −0.95 V (Fig. 4(a)) and −1.10 V (Fig. 4(b)), a current plateau was observed, indicating that the plating process was under diffusion control [21]. Also, a crossover was observed, indicating that deposition occurred by nucleation [22]. Finally, when the sweep was reversed at −1.30 V (Fig. 4(c)), the current increased and nucleation loop was observed, indicating a second nucleation process.

Fig. 5 shows the crossover potentials (E_{cross}) as a function of E_f. It can be seen that for E_f down to −1.25 V, $E_{cross} \sim -0.85$ V and it is independent of E_f. This observed independence, in this potential region, indicates that the nucleation growth mechanism of lead on Pt is under interfacial control. However, beyond $E_f = -1.25$ V, E_{cross} is displaced to more negative potentials. This negative shift for E_{cross} at high E_f is due probably to the

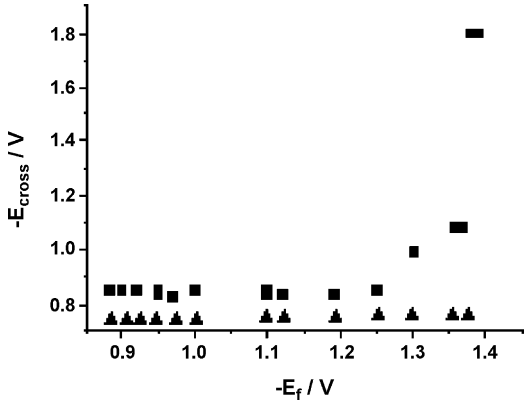

Fig. 5. Values of crossover potentials (E_{cross}) as a function of the reversed potentials (E_f).

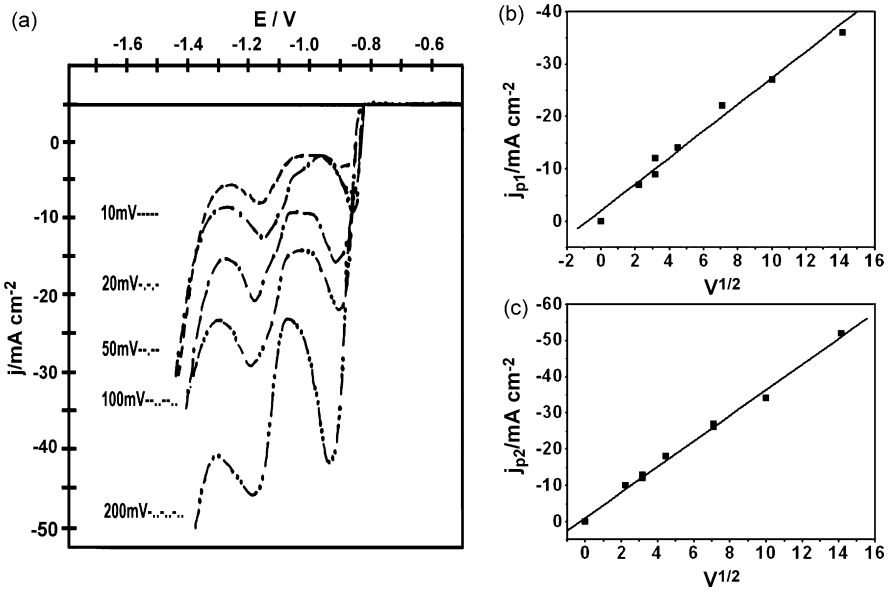

Fig. 6. (a) Voltammetric curves for platinum substrate in 0.05 M $Pb(NO_3)_2$ + 0.05 M $SnCl_2$ + 0.4 M sorbitol + 0.8 M NaOH at various sweep rates (ν/mV s^{-1}): (- - -) 2.0; (· · ·) 5.0; (—) 10; (—·—·—) 20; (—··—··—··) 50; (-·-·-·-·-·-) 100; (-···-···-···) 200. (b) Variation of j_p with $\nu^{1/2}$ for the current peaks in (▲) 1st peak and (■) 2nd peak.

tendency for nucleation growth to fall under diffusion control [22]. Also, another E_{cross} value (∼−0.75 V) was observed for E_f down to ∼−1.40 V. This E_{cross} value relates to the reduction potential $E^{2+}_{Pb}/Pb \sim -0.75$ V (see Fig. 2(b)).

Fig. 6(a) shows the Pb–Sn deposition voltammograms, at different sweep rates (ν). It can be observed that the peak current density increases as the sweep rate increases, suggesting that the deposition process is controlled by mass transport. Fig. 6(b) and (c) shows that current densities (j_p) of peaks c_1 and c_2 increase linearly with $\nu^{1/2}$. The peak current of reduction of Pb(II) and Sn(II) complex species is described by Eq. (1), which includes the reduction of soluble species to form insoluble species [23,24]:

$$j_p = 367 n^{3/2} A C_0 D^{1/2} \nu^{1/2} \quad (1)$$

Considering that in the region of peak c_1 only the Pb(II) complex species is reduced, the diffusion coefficient (D) for this species was calculated from this equation in the region of peak c_1 giving 2.37×10^{-6} cm s^{-1}. This value, as expected, is much smaller than that for hydrated lead ion D_0, 9.8×10^{-6} cm^2 s^{-1} [25]. This is because [Pb(II)/sorbitate] [19] complexes occupy more space than $[Pb(H_2O)_6]^{2+}$ and consequently they have smaller diffusion rates.

In the region of peak c_2, [Pb(II)/sorbitate] and [Sn(II)/sorbitate] complexes were reduced and the diffusion coefficient obtained from Eq. (1) was 1.15×10^{-6} cm s^{-1}, which is smaller than either sodium stannite D_0, 1.84×10^{-6} cm^2 s^{-1} [10], or hydrated lead ion D_0, 9.8×10^{-6} cm^2 s^{-1} [25]. This is because [Pb(II)/sorbitate] and [Sn(II)/sorbitate] complexes are larger than $[Pb(H_2O)_6]^{2+}$ and $[HSnO_2]^-$ ions, respectively, and consequently they have smaller diffusion rates.

3.1. EDS analysis of the Pb–Sn deposits

In order to verify the nature of the deposit at peaks c_1 and c_2 (Fig. 1), analyses by EDS were carried out (Fig. 7(a)–(c) and Table 1).

Fig. 7(a) shows the occurrence of only Pb in the films obtained at deposition potential (E_d) of −0.87 V, with charge density (q_d) of 5.0 C cm^{-2}. A similar result was obtained with 10.0 C cm^{-2}.

Fig. 7(b) and (c) shows the occurrence of both Pb and Sn in the films obtained at −1.17 V with q_d = 5.0 and 10.0 C cm^{-2}, respectively.

It can be seen in Table 1 that when the charge density is changed from 5.0 to 10.0 C cm^{-2} the Sn content in the film obtained at −1.17 V increases from approximately 19 to about 26 wt%. In other words, the composition of films obtained at −1.17 V depends on the amount deposited. Lead is dominant in the alloy obtained at either potential.

Hansen and Anderko [26] summarized the equilibrium phase diagram and reported that the solid solubility of tin in lead is 19.1 wt% at 183 °C.

Sadana and Zhang [27] reported, for alloy electrodeposited from an acid plating bath (pH ∼ 4) at room temperature that the solid solubility of tin in lead was at least 6.8 wt%.

Table 1
Energy dispersive X-ray spectroscopy for electrodeposited films obtained chronoamperometrically

E_p (V)	q_d (C cm^{-2})	Pb (wt%)	Sn (wt%)
−0.87	5.0	100	0
−0.87	10.0	100	0
−1.17	5.0	80.90	19.10
−1.17	10.0	73.65	26.35

E_p: peak potential and q_d: charge density of deposit.

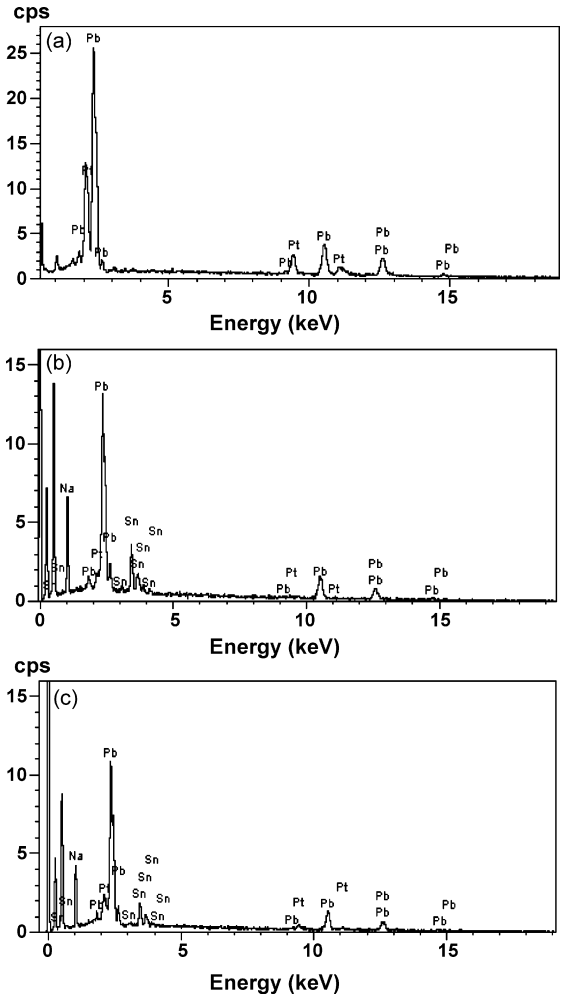

Fig. 7. EDS analysis of Pb–Sn films on Pt substrate obtained chronoamperometrically (a) from −0.500 to −0.870 V, $q_d = 10\,C\,cm^{-2}$, (b) from −0.500 to −1.170 V, $q_d = 10\,C\,cm^{-2}$ and (c) from −0.500 to −1.170 V, $q_d = 5\,C\,cm^{-2}$. Deposition solution: 0.05 M $Pb(NO_3)_2$ + 0.05 M $SnCl_2$ + 0.4 M sorbitol + 0.8 M NaOH.

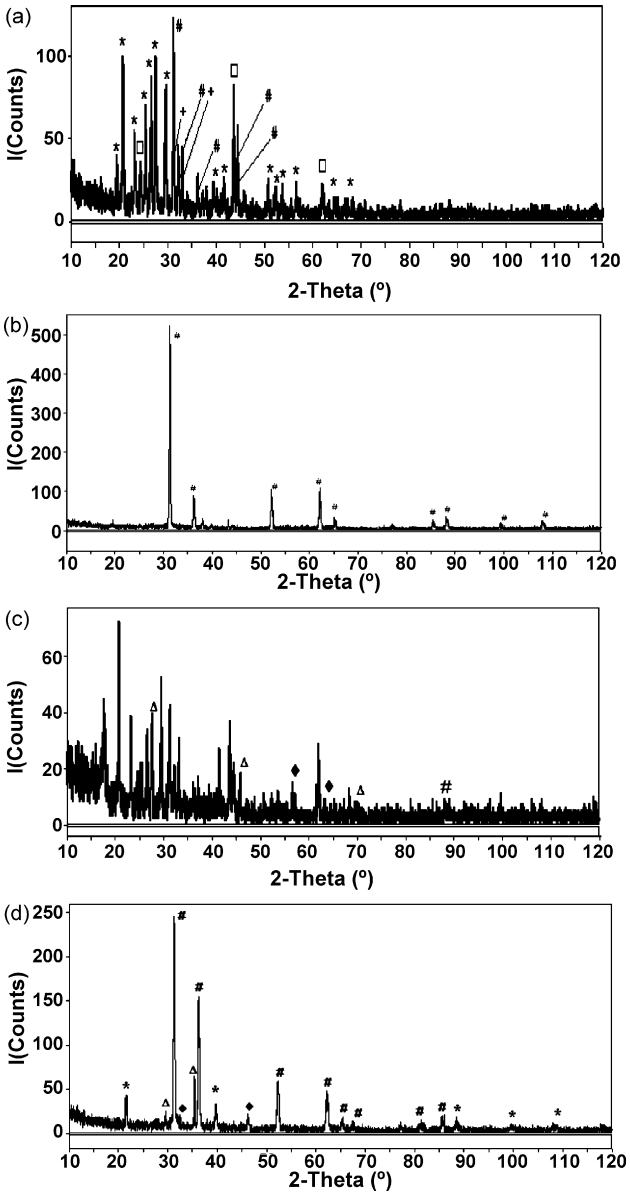

Fig. 8. X-ray diffraction patterns of deposits obtained chronoamperometrically from −0.500 to −0.870 V (a and b) and −0.500 to 1.170 V (c and d), with charge density of $5.0\,C\,cm^{-2}$ (a and c) and $10.0\,C\,cm^{-2}$ (b and d). Deposition solution: 0.05 M $Pb(NO_3)_2$ + 0.05 M $SnCl_2$ + 0.4 M sorbitol + 0.8 M NaOH. Pb (#, JCPDS-04-0686); Pb_2PtO_4 (+, JCPDS-84-1257); $PbPt_4$ (□, JCPDS-06-0463); $PbSnO_3$ (△, JCPDS-17-0607); Sn (♦, JCPDS-04-0673).

Petersson and Ahlberg found that, for equal amounts (10 mM) of Sn^{2+} and Pb^{2+} in the fluorborate plating bath, the content of Sn in the Pb–Sn electrodeposited on gold substrate was ∼2.9 wt% [20] and on glassy carbon substrate was 12 wt% [5].

The solid solubility of tin in lead in the electrodeposited Pb–Sn alloy obtained here from the sorbitol–alkaline plating bath, at −1.17 V and with deposition charge densities of 5.0 and $10.0\,C\,cm^{-2}$, was thus the same as (19 wt%) or higher than (26 wt%) the equilibrium value of 19 wt% Sn reported for thermal alloys [26]. These values (19 or 26 wt% Sn) were also higher than those reported in electrodeposited alloys [27,20].

It can be inferred from these results that at −1.17 V, for both q_d, the co-deposition type was normal [1], since lead predominated in the film.

Finally, it can be concluded from the potentiodynamic curves for the Pt electrode in the Pb, Sn and Pb–Sn plating baths, and also from the EDS analysis of the Pb–Sn deposits, that peak c_1 can be associated with a deposit of Pb, and peak c_2 with a mixed Pb and Sn deposit, the major component being lead.

Petersson and Ahlberg [3] reports that when the amount of tin, in the PbSn film, was higher than 12 wt% Sn the amount of PbO_2 decreases and the overpotential of oxygen evolution increases. Then, the Pb–Sn film obtained at −1.17 V with $q_d = 5.0\,C\,cm^{-2}$ (19 wt% Sn) and $10.0\,C\,cm^{-2}$ (26 wt% Sn), cannot probably be used in lead–acid batteries.

3.2. X-ray analysis of the Pb–Sn deposits

Fig. 8(a)–(d) shows X-ray diffraction patterns of deposits obtained from a solution of Pb and Sn salts, at −0.87 and −1.17 V, with $q_d = 5.0$ and $10.0\,C\,cm^{-2}$ for both E_d.

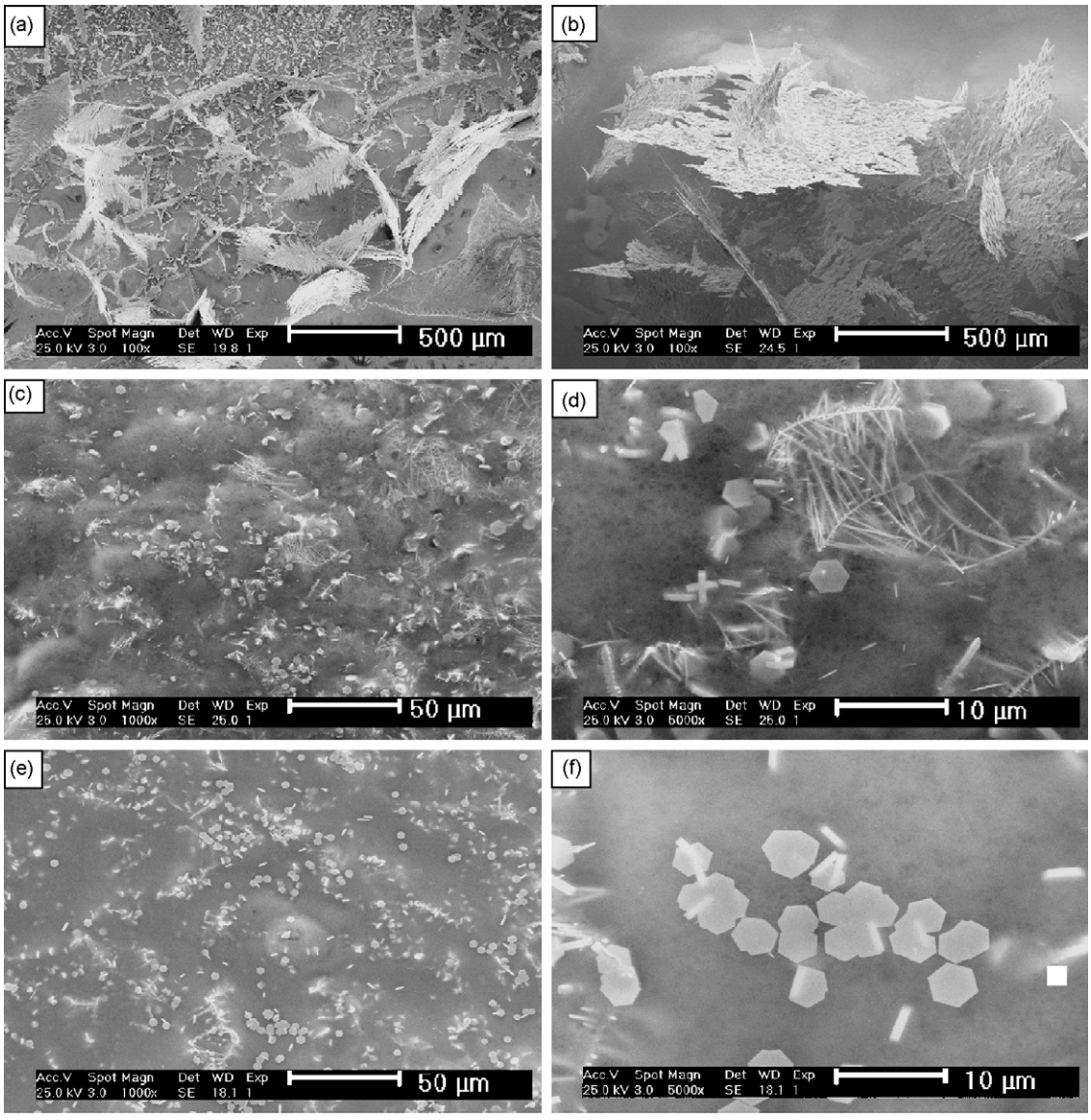

Fig. 9. SEM micrographs of Pb–Sn films obtained chronoamperometrically: (a) from −0.500 to −0.870 V, $q_d = 5\,C\,cm^{-2}$; (b) from −0.500 to −0.870 V, $q_d = 10\,C\,cm^{-2}$; (c and d) from −0.500 to −1.170 V, $q_d = 5\,C\,cm^{-2}$; (e and f) from −0.500 to −1.170 V, $q_d = 10\,C\,cm^{-2}$. Deposition solution: 0.05 M $Pb(NO_3)_2$ + 0.05 M $SnCl_2$ + 0.4 M sorbitol + 0.8 M NaOH.

The diffractograms from the deposits obtained at −0.87 V with $q_d = 5.0\,C\,cm^{-2}$ (Fig. 8(a)) or $q_d = 10.0\,C\,cm^{-2}$ (Fig. 8(b)) indicated the presence of Pb, Pb_2PtO_4 and $PbPt_4$ and absence of Sn [28]. However, those obtained at −1.17 V with $q_d = 5.0\,C\,cm^{-2}$ (Fig. 8(c)) or $q_d = 10.0\,C\,cm^{-2}$ (Fig. 8(d)) showed some peaks that could readily be assigned to Pb, β-Sn, and $PbSnO_3$ [28]. These results are consistent with the EDS finding that Pb alone (Fig. 7(a)) and Pb and Sn (Fig. 7(b) and (c)) were obtained at −0.87 and −1.17 V, respectively.

3.3. Scanning electronic microscopy

SEM analysis was carried out on Pb–Sn layers formed from a solution of Pb and Sn salts, at −0.87 and −1.17 V, with 5.0 and $10.0\,C\,cm^{-2}$ for both E_d (Fig. 9(a)–(f)).

Comparing these micrographs, it can be observed that the Pb–Sn layers had dissimilar morphologies. It may be noted, at −0.87 V and for both q_d (Fig. 9(a) and (b)), that dendritic crystallites were scattered over an adherent initial layer on the electrode. This initial layer on the Pt substrate was seen by the naked eye and it could only be removed from the platinum electrode when immersed in concentrated sulphuric–nitric acid solution, i.e., we could not remove this layer wiping with paper.

These results accord with the fact that the deposition process is limited by diffusion and, consequently, protuberant regions of surface grow faster, since they are more accessible, leading to dendritic deposits. This structure was not retained when tin was co-deposited with lead (Fig. 9(c)–(f)). In Fig. 9(c) and (d), Pb–Sn film obtained at −1.17 V with $5.0\,C\,cm^{-2}$ can be seen, composed mainly of hexagonal crystallites and only a few dendrites, both dispersed over an initial layer of deposit. However,

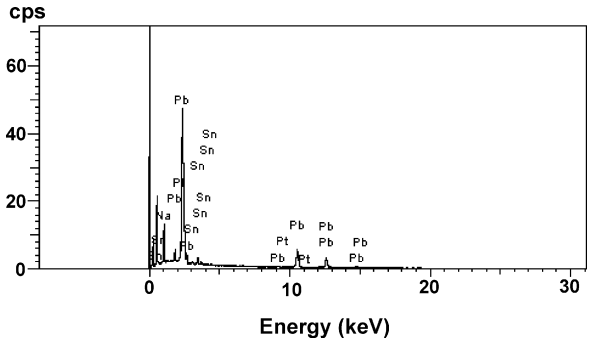

Fig. 10. EDS analysis of hexagonal crystallite of Pb–Sn film on substrate platinum obtained chronoamperometrically from −0.500 to −1.170 V, $q_d = 10\,C\,cm^{-2}$. Deposition solution: 0.05 M $Pb(NO_3)_2$ + 0.05 M $SnCl_2$ + 0.4 M sorbitol + 0.8 M NaOH.

for $10.0\,C\,cm^{-2}$ (Fig. 9(e) and (f)), the dendrite crystallites cannot be observed. This is probably due to the higher proportion of tin in the layer.

EDS analysis carried out on a hexagonal crystallite of the Pb–Sn layer obtained at −1.17 V with $10\,C\,cm^{-2}$ showed that the content of Sn was 6.28 wt% and of Pb, 93.72 wt% (Fig. 10).

These results are significant, since they show that when Sn was present in the layer, dendritic growth of the deposit was hindered.

Petersson and Ahlberg [5,20] observed by SEM that in the presence of lead, the deposition of tin on tin is inhibited and also the formation of dendrites is prevented.

4. Conclusions

Lead and lead–tin were electrodeposited on Pt substrates from a sorbitol–alkaline solution, at −0.87 and −1.17 V, respectively, as suggested by voltammetric curves and confirmed by EDS and XRD analysis. The deposition process occurred by nucleation and the growth was controlled by mass transport.

For E_f down to −1.25 V, the E_{cross} value was ∼−0.85 V and it was independent of E_f, but beyond −1.25 V it shifted to more negative values, indicating that the nucleation growth mechanism of lead onto Pt was at first under interfacial control and then, at more negative E_f, it fell under diffusion control. The E_{cross} value (∼−0.75 V) observed for E_f down to ∼−1.40 V relates to the reduction potential $E^{2+}_{Pb}/Pb \sim -0.75$ V.

From the SEM results it can be inferred that co-deposition of tin with lead hinders the development of dendritic crystals. EDS analysis showed that doubling the q_d increased the Sn content in the deposits obtained at −1.17 V. X-ray analysis of the deposits obtained at −0.87 or −1.17 V, with $q_d = 5.0$ and $10.0\,C\,cm^{-2}$ for both E_d, suggests the presence of a mixture of Pb, $PbPt_4$ and Pb_2PtO_4 at −0.87 V or Pb, β-Sn, and $PbSnO_3$ at −1.17 V.

Acknowledgements

Financial support from the Brazilian research foundations: CNPq and FAPESP (Proc. no 04/14142-2) are gratefully acknowledged.

References

[1] A. Brenner, Electrodeposition of Alloys. Principles and Practice, vol. 1, Academic Press, New York, 1963.
[2] D. Pavlov, J. Power Sources 42 (1993) 345–363.
[3] I. Petersson, E. Ahlberg, J. Power Sources 91 (2000) 143–149.
[4] F.A. Lowenheim, Modern Electroplating, John Wiley, New York, 1963.
[5] I. Petersson, E. Ahlberg, J. Electroanal. Chem. 485 (2000) 166–177, Part I.
[6] N.V. Parthasaradhy, Practical Electroplating Handbook, Prentice Hall, New Jersey, 1989.
[7] E.J. Roehl, US Patent No. 2,734,025 (1956).
[8] E.J. Roehl, Iron Age 173 (1954) 140–142.
[9] E.M. Oliveira, I.A. Carlos, Surf. Coat. Technol. 200 (2006) 5978.
[10] R.L. Broggi, G.M. de Oliveira, L.L. Barbosa, E.M.J.A. Pallone, I.A. Carlos, J. Appl. Electrochem. 36 (2006) 403–409.
[11] M.S. Pereira, L.L. Barbosa, C.A.C. Souza, A.C.M. de Moraes, I.A. Carlos, J. Appl. Electrochem. 36 (2006) 727.
[12] L.L. Barbosa, I.A. Carlos, Surf. Coat. Technol. 201 (2006) 1695–1703.
[13] I.A. Carlos, L.L. Barbosa, M.R.H. de Almeida, G.M. Oliveira, M. Yonashiro, R.M. Carlos, Surf. Coat. Technol. 192 (2005) 145–153.
[14] I.A. Carlos, T.T. Matsuo, J.L.P. Siqueira, M.R.H. de Almeida, J. Power Sources 132 (2004) 261–265.
[15] I.A. Carlos, E.M. Oliveira, G.A. Finazzi, Surf. Coat. Technol. 187 (2004) 377–387.
[16] I.A. Carlos, M.R.H. Almeida, J. Electroanal. Chem. 562 (2004) 153–159.
[17] I.A. Carlos, J.L.P. Siqueira, G.A. Finazzi, M.R.H. de Almeida, J. Power Sources 117 (2003) 179–186.
[18] A.R. Despic, V.D. Jovic, in: R. White, et al. (Eds.), Modern Aspects of Electrochemistry, No. 27, Plenum Press, New York, 1995.
[19] J.L.P. Siqueira, Mr. Dissertation, Universidade Federal de São Carlos, Brasil, 2003.
[20] I. Petersson, E. Ahlberg, J. Electroanal. Chem. 485 (2000) 178–187, Part II.
[21] A.J. Bard, L.R. Faulkner, Electrochemical Methods: Fundamentals and Applications, John Wiley & Sons, New York, 1980.
[22] S. Fletcher, C.S. Halliday, D. Gates, M. Westcott, T. Lwin, G. Nelson, J. Electroanal. Chem. 159 (1983) 267.
[23] T. Berzins, P. Delahay, J. Am. Chem. Soc. 75 (1953) 555.
[24] G. Mamantov, D.L. Manning, J.M. Dale, J. Electroanal. Chem. 9 (1965) 253.
[25] I.M. Kolthoff, J.J. Lingane, Polarography 1, Interscience Publishers Inc., New York, 1952.
[26] M. Hansen, K. Anderko, Constitution of Binary Alloys, 2nd ed., McGraw Hill, New York, 1958, p. 1106Y.
[27] Y.N. Sadana, Z.H. Zhang, Surf. Coat. Technol. 38 (1989) 299–310.
[28] Joint Committee on Powder Diffraction Standards, JCPDS in: International Centre for Diffraction Data, Powder Diffraction File-PDF-2, Database Sets 1–49, Pennsylvania, ICDD, 2000 (CDROM).